J. CHEM. SOC. FARADAY TRANS., 1991, 87(17), 2821–2828

Carbon Dioxide Hydrogenation over Au/ZrO_2 Catalysts from Amorphous Precursors: Catalytic Reaction Mechanism

Rene A. Koeppel and Alfons Baiker
Department of Chemical Engineering and Chemical Technology, Swiss Federal Institute of Technology, ETH Zentrum, CH-8092 Zürich, Switzerland
Christoph Schild and Alexander Wokaun*
Physical Chemistry II, University of Bayreuth, P.O. Box 101251, D-8580 Bayreuth, Germany

An active catalyst for carbon dioxide hydrogenation is obtained by exposing an amorphous $Au_{25}Zr_{75}$ alloy to CO_2 hydrogenation conditions. During this *in situ* activation, metallic gold particles of 8.5 nm mean size are formed, and the zirconium component of the catalyst is oxidized to ZrO_2. For comparison, a further Au/ZrO_2 catalyst was synthesized by coprecipitation, followed by calcination of the amorphous precipitate. The calcination step strongly enhances the activity of the catalyst; gold segregation and zirconia crystallization are found to occur in this process. The structural and chemical changes are characterized by gas adsorption, X-ray diffraction and thermal analysis.

The main products of CO_2 hydrogenation over these catalysts, as identified by gas chromatography, are methanol and CO. To investigate the reaction mechanism, diffuse reflectance FTIR spectroscopy has been used. Observed surface species are correlated with the formation of gas-phase products. Adsorption of CO_2–H_2 results in rapid formation of formate as the primary surface intermediate; two types of formate species are clearly detected on the coprecipitated catalyst, and are assigned by means of formic acid adsorption experiments. CO formation from CO_2 appears to proceed *via* surface carbonate, in a surface reaction that corresponds to a 'basic variant' of the reverse water-gas-shift reaction. The CO formed in this process is, in turn, the starting point for a series of surface hydrogenation steps that yield π-bonded formaldehyde, surface-bound methylate and finally methanol. This sequence of reactions is confirmed by separate CO–H_2 adsorption experiments.

Significant progress in the preparation of catalysts from glassy metal–zirconium alloy precursors has been achieved in the past few years.† Glassy alloys in their as-quenched state generally exhibit low catalytic activity owing to the very low intrinsic specific surface area (< 1 m^2 g^{-1}). However, various efficient catalysts have been prepared by exposing these alloys to atmospheres containing an oxygen source (*e.g.* O_2, CO_2, H_2O).[1] The activation treatment is typically performed at temperatures that are considerably lower than the crystallization temperature of the alloys. During this exposure, a series of solid-state transformations occur, which generally include the preferential oxidation of the more electrophilic constituents (*e.g.* Zr, B, P), and segregation or precipitation of catalytically active metal particles (*e.g.* Fe, Cu, Pd, Au).[2–7] These transformations are accompanied by drastic changes in the textural and surface properties of the materials. A special structural feature of catalysts prepared by these procedures is the intimate contact between the metal and the oxidic matrix. The resulting large interfacial area leads to catalytic activities that can exceed those of conventionally prepared catalysts by orders of magnitude.[8]

Concerning the Au/ZrO_2 system, only a single investigation of carbon monoxide hydrogenation over a catalyst derived from amorphous $Au_{25}Zr_{75}$ has been reported to date.[2] In recent studies[3–7] of activated metal–zirconium catalysts we have shown that carbon dioxide is also an effective starting material for methanol and methane production. Over Cu/ZrO_2,[3,4] methanol is the primary CO_2 hydrogenation product; with Pd/ZrO_2, methane is produced in addition, depending on the reaction conditions.[5,6] Over Ni/ZrO_2 catalysts, methane is exclusively formed when starting from CO_2–H_2 mixtures.[7]

An important aim of our surface spectroscopic investigations is the elucidation of reaction mechanisms for catalytic CO_2 and CO hydrogenation reactions under a set of defined reaction conditions. Recent experiments[9] indicate that the selectivity behaviour of the various metals does not support a proposal by Frost,[10] which stated that the work function of the metal was crucial in determining the Schottky barrier height, whereas the intrinsic electronic properties and surface chemistry of the supported metals were of lesser importance. Data collected and interpreted in the present report with Au/ZrO_2 catalysts provide further information on the hydrogenation mechanisms, which complements the results obtained with transition metal–zirconia and other group IB metal–zirconia catalysts.

† For comprehensive reviews, see *e.g.* ref. 1.

Experimental

Catalysts

The amorphous $Au_{25}Zr_{75}$ alloy used as a catalyst precursor was prepared by the conventional melt-spinning technique from the premixed melt of the pure metals. The resulting ribbons, of 20–30 μm thickness, were ground under liquid nitrogen to flakes of 0.1 –1 mm in size before use. X-Ray diffraction indicated that the bulk of the ground metallic glass was still amorphous; part of the surface was oxidized during exposure to air, as indicated by the dark grey colour of the ribbons. The B.E.T. surface area of the material was *ca.* 0.2 m^2 g^{-1}, as measured by krypton adsorption at 77 K.

A conventionally prepared Au/ZrO_2 catalyst was used as a reference. The catalyst, containing 5 wt.% gold, was synthesized by coprecipitation at constant pH and temperature. Aqueous solutions of $HAuCl_4/ZrO(NO_3)_2$ and NaOH/sodium formate were slowly and simultaneously added into deionized water at 363 K, with vigorous stirring. During this procedure, a pH of 7 was maintained. Subsequently, the resulting suspension was stirred at 363 K for 15 min, and then filtered off. The precipitate was thoroughly washed with deionized water and finally with methanol, and dried at

393 K *in vacuo* for 15 h. After calcination in air at 723 K for 3 h, the material was crushed to a grain size of 50–150 μm.

The preparation procedures of the amorphous zirconia and the impregnated Pd/ZrO_2 catalyst employed in the formic acid adsorption experiments have been reported in detail elsewhere.[11]

Catalyst Characterization

Structural and chemical properties of the amorphous $Au_{25}Zr_{75}$ alloy, as well as the final catalyst, were characterized by means of X-ray diffraction (XRD), gas adsorption (nitrogen and krypton) and thermal analysis (TG/DTA). X-Ray analysis was performed on a powder diffractometer (Philips PW 1700), using Cu-$K\alpha$ radiation. Mean crystallite sizes were estimated from the half-width of the Au(111) reflexes, using the Scherrer equation. The measured peak width was corrected for instrumental broadening using the function proposed by Warren.[12]

Surface areas ($S_{B.E.T.}$) were calculated using a cross-sectional area of 0.163 nm^2 for nitrogen and 0.195 nm^2 for the krypton atom.[13] Pore size distributions were determined according to the B.J.H. method,[14] using the equation of Halsey.[15]

Thermal analysis experiments were carried out on a Mettler 2000C thermoanalyser in different gas atmospheres; a heating rate of 10 K min^{-1} was employed.

Catalytic Tests

Catalytic activity tests were performed in a continuous tubular flow fixed-bed microreactor operated at 1.7 MPa. Details of the apparatus have been reported in ref. 3. Feed and product gases were analysed in a gas chromatograph (HP, model 5890A) equipped with a thermal conductivity detector. Products were separated in a stainless-steel column (5 m, 1/8 in i.d.) containing 80–100 mesh Poropak QS.

Experiments were carried out using 1.0 g of catalyst and a reactant flow rate of 90 cm^3 min^{-1} (STP) of CO_2–H_2 (1 : 3), in the temperature range 413–533 K. The reactant gases, CO_2 (99.9%) and H_2 (99.999%), were fed from high-pressure cylinders without further purification.

The amorphous $Au_{25}Zr_{75}$ alloy was activated by exposure to reaction conditions at a temperature of 493 K.

Spectroscopic Measurements

The hydrogenation reactions were monitored by diffuse reflectance spectroscopy under defined reaction conditions. Spectra were recorded on an FTIR instrument (Perkin-Elmer, model 1710) equipped with a controlled environmental chamber (Spectra Tech); temperature in this chamber was controlled to within ±2 K. The spectrometer and temperature controller were connected to a personal computer (Nixdorf, AT 386) for data handling and processing.

The gas-dosing system was designed to introduce three gases independently into the reaction chamber. Gas flows were adjusted to the desired values using volume flow controllers (Rota). CO_2 (99.9993%), CO (99.997%), and H_2 (99.999%) were used without further purification. Before the FTIR measurements, the catalysts, which had been stored under atmospheric conditions, were reactivated in hydrogen flow at elevated temperatures (450–500 K) for several hours.

After catalyst reactivation, the background spectrum was recorded at an appropriate temperature in the range to be studied during the following catalytic reactions (*e.g.* at 423K for the range 373–473 K). A defined mixture of the gaseous reactants, with the desired pre-adjusted composition, was either passed continuously over the sample ('dynamic experiments'), or enclosed in the reaction chamber ('static system') at total pressures of *ca.* 3 × 10^5 Pa. Surface reactions were monitored by recording time-resolved or temperature-dependent DRIFT spectra, respectively. Typically, 50–250 scans at a resolution of 8 cm^{-1} have been accumulated.

Reference adsorption experiments were performed by directing the nitrogen carrier-gas stream through a sealed flask containing formic acid (Merck, 98–100%) for a defined period of time. Subsequent to the adsorption of the HCO_2H pulse, changes in the surface spectra were monitored as a function of time or temperature, as detailed below.

Results

Catalytic Tests and Effects of Thermal Pretreatment

Differential thermal analysis (DTA) and thermogravimetric (TG) measurements of the amorphous $Au_{25}Zr_{75}$ alloy in the reaction gas mixture (CO_2–H_2) at atmospheric pressure gave evidence for a reaction occurring in the temperature range 483–800 K, and resulting in the formation of metallic gold and zirconia. By comparative measurements in an argon atmosphere, crystallization was shown to occur between 850 and 900 K, which is significantly higher than the activation temperature of 493 K.

Changes in the catalytic behaviour of the amorphous precursor during its transformation to the final catalyst are presented as a function of time-on-stream in Fig. 1. The time dependence of the product concentrations was used to monitor the activation process. A marked increase of the CO_2 conversion rate was detected during the initial period of activation, to approach a 'steady-state' conversion after *ca.* 7 h. After a constant activity level had been reached, water, CO and methanol were identified as the major products, besides smaller amounts of methane. Note that during the early stages of activation, water production was less than expected from the CO_2 conversion. Detectable concentrations of methane were produced after 3 h on stream.

The selectivity behaviour of the Au/ZrO_2 catalyst derived from amorphous $Au_{25}Zr_{75}$, and the corresponding data obtained for the conventionally prepared Au/ZrO_2 catalyst, are compared in Fig. 2. Steady-state selectivities of the two catalyst systems at different temperatures are presented as a function of CO_2 conversion. Qualitatively, both catalysts exhibit similar characteristics. CO and, to a lesser extent,

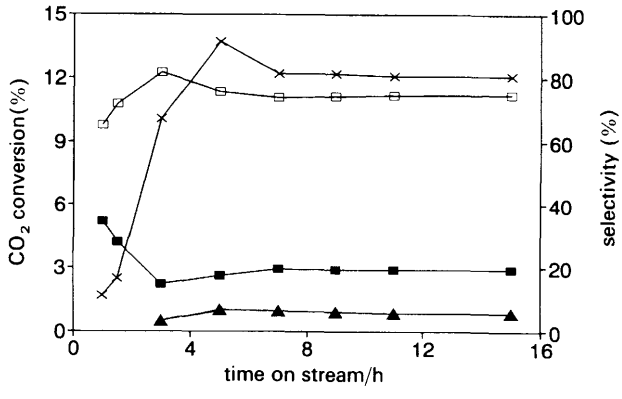

Fig. 1 Changes in the activity of an amorphous $Au_{25}Zr_{75}$ alloy during *in situ* activation at T = 493 K and p = 17 bar. CO_2 conversion and selectivities are monitored as a function of time on stream. Further reaction conditions are specified in the experimental part. ×, conversion; ■, methanol selectivity; □, carbon monoxide selectivity; ▲, methane selectivity

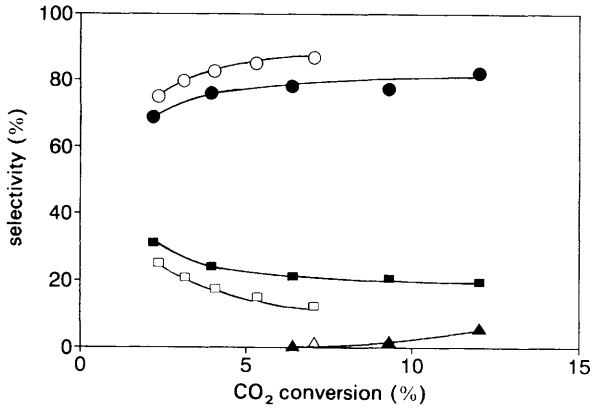

Fig. 2 Dependence of product selectivities for the catalyst obtained by *in situ* activation of amorphous $Au_{25}Zr_{75}$ (filled symbols), and for the 5 wt.% Au/ZrO_2 catalyst prepared by coprecipitation (open symbols), on CO_2 conversion under steady state conditions (□, ■, methanol; ○, ●, carbon monoxide; △, ▲, methane). The conversion scale represents a temperature range from 413 to 493 K for $Au_{25}Zr_{75}$, and from 493 to 533 K for Au/ZrO_2

methanol are formed as the main products; the selectivity towards CO increases slightly with CO_2 conversion. The catalyst derived from amorphous $Au_{25}Zr_{75}$ shows a constantly higher methanol selectivity than the conventionally prepared one, when referenced to the same CO_2 conversion.

Comparatively little methane is produced even at high CO_2 conversion rates. Note that over the catalyst derived from the amorphous alloy, significantly lower temperatures are required to reach acitivities comparable to those of the conventionally prepared Au/ZrO_2; at 493 K, the CO_2 conversion rates differ by *ca.* on order of magnitude.

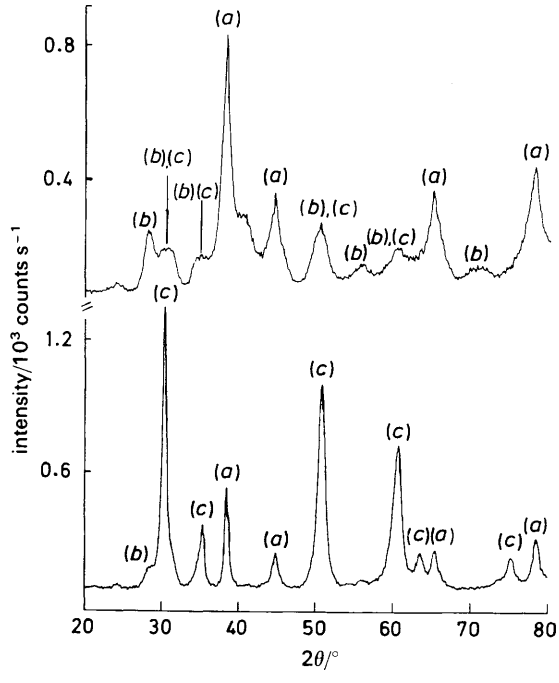

Fig. 3 X-Ray diffraction patterns (Cu-Kα) of the catalyst obtained by *in situ* activation of the amorphous $Au_{25}Zr_{75}$ alloy at 493 K in CO_2–H_2 (upper trace), and of the coprecipitated 5 wt.% Au/ZrO_2 catalyst after CO_2 hydrogenation (lower trace). Assignment of the reflections: (*a*) Au; (*b*) monoclinic ZrO_2; (*c*) tetragonal ZrO_2. Note that in the upper trace some reflections are overlapping

Chemical and Textural Properties

The transformation of the initially amorphous $Au_{25}Zr_{75}$ precursor into the final catalytic system results in the formation of crystalline metallic gold particles and less ordered zirconium dioxide, as evidenced by the X-ray diffractogram shown in Fig. 3 (upper trace). The crystalline fraction of zirconium dioxide adopts predominantly the structure of the monoclinic modification. The gold particles have a mean size of *ca.* 8.5 nm, as estimated from the line broadening of the Au (111) reflection.

Prior to calcination, the coprecipitated Au/ZrO_2 catalyst is characterized by the presence of crystalline gold particles (13.5 nm mean diameter), in addition to an X-ray amorphous zirconia phase. Calcination at 723 K in air results in the crystallization of the initially amorphous zirconia. DTA measurements of the uncalcined catalyst in air and hydrogen–argon (5% H_2) yield the same crystallization temperature of the amorphous zirconia (715 K) both under oxidizing and reducing conditions. In the XRD pattern of the coprecipitated, calcined sample after exposure to CO_2 hydrogenation conditions (Fig. 3, lower trace), zirconia appears predominantly in the tetragonal modification, with a smaller monoclinic fraction. The mean size of the gold particles has increased slightly to *ca.* 15 nm.

The chemical changes occurring during *in situ* activation of the amorphous $Au_{25}Zr_{75}$ are accompanied by drastic changes in the textural properties of the catalyst. The B.E.T. surface area of the precursor alloy increases from *ca.* 0.3 to 47 $m^2\ g^{-1}$ during the transformation process. Pore size distributions calculated from the desorption branch of the nitrogen isotherms indicate that the final catalyst contains pores of *ca.* 2 nm mean size. Hysteresis was observed only to a small extent in the range $p/p_0 > 0.9$, which points to the presence of some larger cracks. Indications for microporosity also emerged from the shape of the adsorption isotherm (type I according to BDDT classification[16]) and from calculated *t*-plots,[17] which suggest the presence of slit-like micropores. These observations hint to a similar structure as has been recently found for a Pd/ZrO_2 catalyst derived from Pd_1Zr_2 alloys.[8] This catalyst exhibited thin plate-like agglomerates that contained intimately mixed palladium and zirconia domains (*cf.* ref. 8, Fig. 7).

Calcination of the conventionally prepared Au/ZrO_2 catalyst led to a drastic decrease in the B.E.T. surface area, from an initial value of 206 to a surface of 83 $m^2\ g^{-1}$ for the catalysts used under CO_2 hydrogenation conditions. The nitrogen isotherm of the calcined sample was of type IV (BDDT classification) and exhibited a type H4 shaped hysteresis loop (IUPAC classification), indicating the presence of a well developed mesoporous system.[16] Mesopore size distributions calculated from the desorption branch of the isotherm showed the presence of a pore size maximum at 3.6 nm, with no indication of microporosity.

Spectroscopic Measurements

The assignment of the vibrational bands reported in the following section is based on our recent studies with Pd/ZrO_2 and Cu/ZrO_2 catalysts.[4,6] Extensive adsorption experiments of reference compounds have been performed,[4] and a table assigning the various observed bands has been given.[6] For convenience, the most important vibrational frequencies of surface species are summarized in Table 1 and compared with the results of the present report as well as literature data.

The catalytic reactions of a static CO_2–H_2 mixture (1 : 4 by volume) were investigated by FTIR spectroscopy as a func-

Table 1 Assignment of vibrational absorptions of various surface species

vibration	molecule	observed frequencies, ν/cm^{-1} present study	literature	ref.
ν(C—O)	CH_3O^-	1040–1050	1010–1090	4, 6, 18
ν(C—O)	η^2-CH_2O	1145	1140–1165	4, 6
ν(C—O)$_a$	CO_3^{2-}(b)[a]	1220–1300	1260–1310	19,20
ν(C—O)$_s$	CO_3^{2-}(m)[a]	1350–1400	1330–1390	19, 20
ν(C—O)$_s$	HCO_2^-	1360 (type II) 1380 (type I)	1360–1390	4, 6, 21
ν(C—O)$_s$	CO_3^{2-}(m)[a]	1400–1450	1420–1540	19,20
ν(C—O)$_a$	HCO_2^-	1580 (type I) 1600 (type II)	1570–1590	4, 6, 21
ν(C=O)	CO_3^{2-}(b)[a]	1630–1680	1590–1670	19, 20
ν(C—O)$_s$ + δ(C—H)	HCO_2^-	2750	2750	21
ν(C—H)$_s$	CH_3O^-	2820	2820–2830	4, 6, 21
ν(C—H)	HCO_2^-	2880	2870–2880	4, 6, 21
ν(C—H)$_a$	CH_3O^-	2930	2930–2950	4, 6, 21
ν(C—O)$_a$ + δ(C—H)	HCO_2^-	2960	2950, 2960	21, 22

[a] m = monodentate, b = bidentate surface carbonate.

tion of surface temperature over the catalyst derived from amorphous $Au_{25}Zr_{75}$ (Fig. 4). CO and H_2O, *i.e.* the products of the reverse water-gas-shift (RWGS) reaction, are observed over the whole temperature range studied, as evidenced by the doublet centred at 2150 cm^{-1} due to ν(C—O) of CO(g) and the multiplet around 1620 cm^{-1} due to δ(HOH) of gaseous water, respectively. At temperatures higher than *ca.* 473 K, methane is formed in addition, with ν(C—H) at 3014

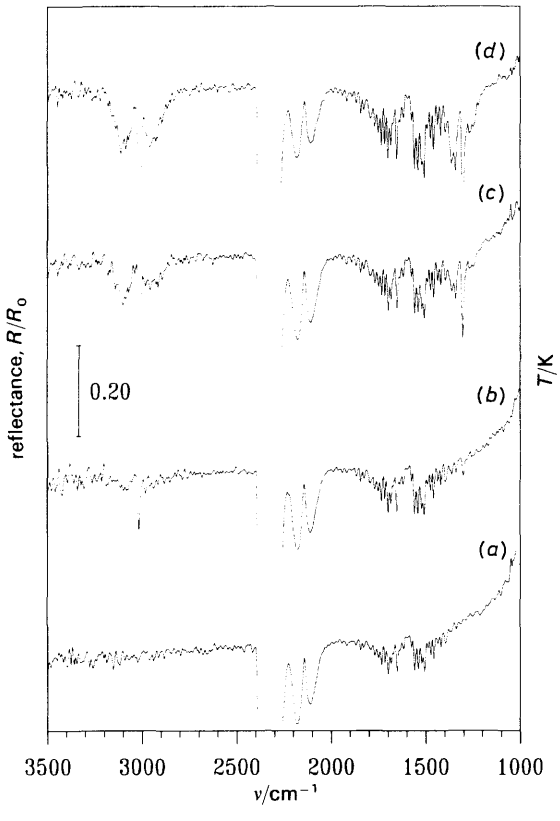

Fig. 4 Temperature dependence of CO_2 hydrogenation reactions over a catalyst derived from the amorphous $Au_{25}Zr_{75}$ alloy. The surface is exposed to a static CO_2–H_2 (1 : 4) mixture at p = 3.5 bar. Diffuse reflectance FTIR (DRIFT) spectra are recorded while the temperature is being raised: (*a*) 443, (*b*) 473, (*c*) 503 and (*d*) 533 K.

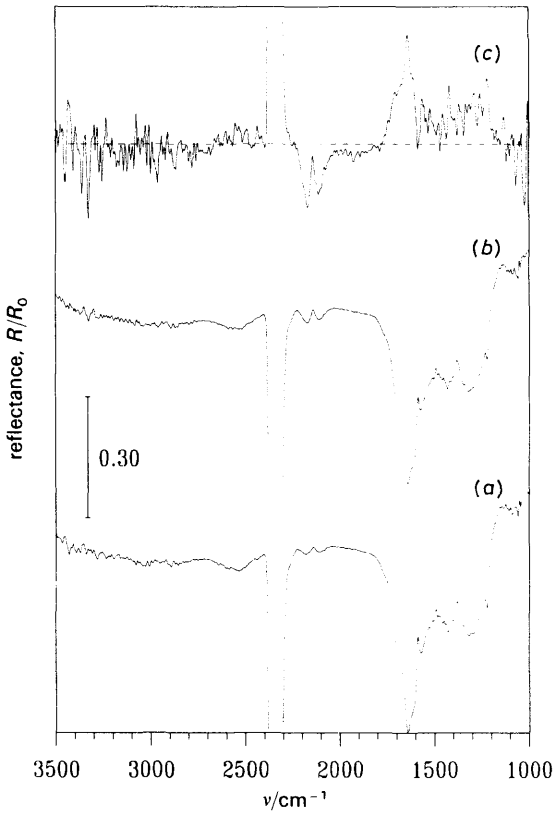

Fig. 5 Surface reactions during CO_2 hydrogenation over the 5 wt.% Au/ZrO_2 catalyst (prepared by coprecipitation) at 403 K (*a*) after 5 min, (*b*) after 15 min. The surface is exposed to a static CO_2–H_2 (1 : 4) mixture at p = 3.5 bar. Time-dependent changes in the DRIFT spectra are made evident in the difference spectrum shown in the upper trace (*c*). This spectrum has been plotted on a six times expanded ordinate scale; zero difference is indicated by the dashed line

cm^{-1} and δ(C—H) at 1308 cm^{-1}, in agreement with the results presented in Fig. 1. No bands due to adsorbed surface species are detected besides the mentioned gas-phase signals; this fact parallels our observations obtained with other catalysts derived from amorphous precursors, such as $Pd_{25}Zr_{75}$ [6] and $Ni_{64}Zr_{36}$.[7]

As found with the catalytic systems investigated in ref. 6 and 7, there are large differences between the alloy-derived and the conventionally prepared catalysts with regard to surface species: For the coprecipitated Au/ZrO_2 catalyst, large amounts of surface carbonates and formate are formed from a CO_2–H_2 reaction mixture at 403 K (Fig. 5), as evidenced by the broad bands between 1700 and 1200 cm^{-1} (*cf.* Table 1). Furthermore, the concentration of bidentate surface carbonate slightly decreases with time, while gaseous CO is being formed. This fact will be discussed below as an indication for the 'basic' RWGS reaction. At higher temperatures, the rate of surface formate production is strongly increased (bands at 2880, 1600–1580 and 1390–1360 cm^{-1}), while the concentration of bidentate carbonate further decreases (1630 and 1200–1300 cm^{-1} vibrations); CO(g) is continuously being formed (Fig. 6). At the highest temperature under investigation, *i.e.* 523 K, surface formate is still produced; its total surface coverage reaches such a high level that even signals from combination vibrations are visible in the spectrum (bands at 2960 and 2750 cm^{-1} in Fig. 7). Note that the band around 1600 cm^{-1} (HCO_2^-, asymmetric stretching vibration) appears split, which points to the presence of two kinds of surface formate (see below). Gaseous water from the RWGS

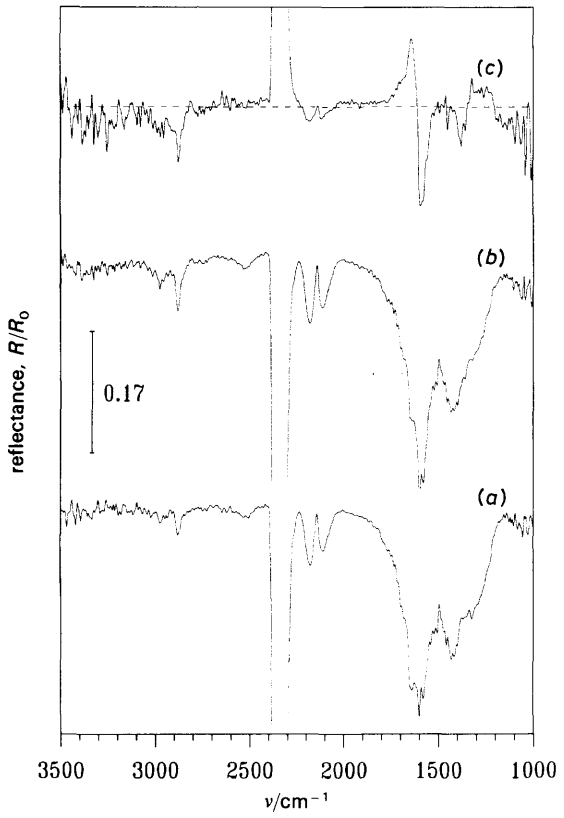

Fig. 6 Surface reactions during CO_2 hydrogenation over the 5 wt.% Au/ZrO_2 catalyst (prepared by coprecipitation) at 483 K (*a*) after 5 min, (*b*) after 15 min. The surface is exposed to a static CO_2–H_2 (1 : 4) mixture at $p = 3.5$ bar. Time-dependent changes in the DRIFT spectra are made evident in the difference spectrum shown in the upper trace (*c*). This spectrum has been plotted on a two times expanded ordinate scale; zero difference is indicated by the dashed line

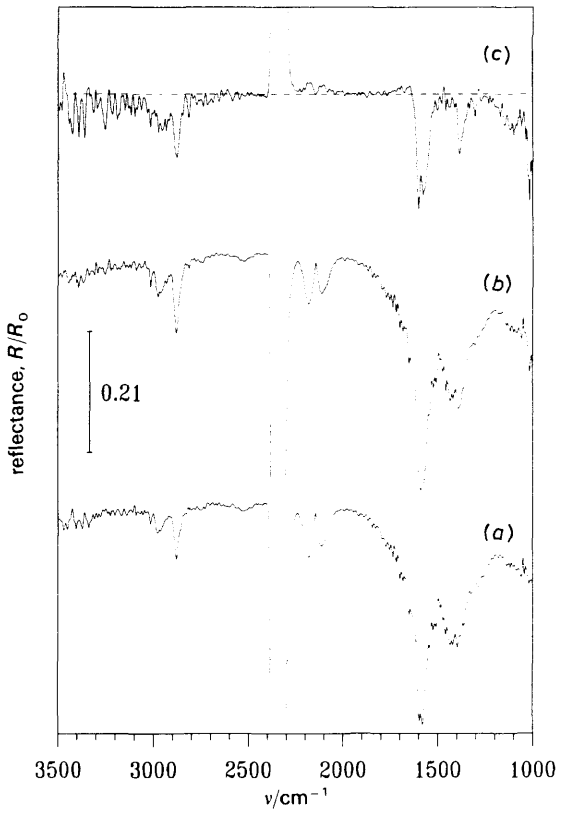

Fig. 7 Surface reactions during CO_2 hydrogenation over the 5 wt.% Au/ZrO_2 catalyst (prepared by coprecipitation) at 523 K (*a*) after 5 min, (*b*) after 15 min. The surface is exposed to a static CO_2–H_2 (1 : 4) mixture at $p = 3.5$ bar. Time-dependent changes in the DRIFT spectra are made evident in the difference spectrum shown in the upper trace (*c*). This spectrum has been plotted on a two times expanded ordinate scale; zero difference is indicated by the dashed line

reaction, which is accumulated in the reaction chamber, gives rise to the weak multiplet of bands centred around 1600 cm^{-1}, which is discerned on both sides of the respective formate peak [Fig. 7(*a*) and (*b*)].

Weak absorptions are observed between 1000 and 1200 cm^{-1} in the spectrum taken after 15 min, as well as in the difference spectrum [Fig. 7, (*b*) and (*c*)]. These signals, which have been assigned[6] to π-bonded formaldehyde (1145 cm^{-1}) and surface methylate (1050 cm^{-1}), respectively, grow in intensity if a CO_2–H_2 flow is passed over the sample for longer times [Fig. 8(*a*)]. Simultaneously, C—H stretching vibrations at 2930 and 2820 cm^{-1} appear in the spectrum, which are characteristic for the methyl group in methylate and/or methanol. When starting from CO–H_2 [Fig. 8(*b*)], there is a further substantial increase of these bands. These results are in excellent agreement with our recent observations over Cu/ZrO_2 and Pd/ZrO_2 catalysts:[4,6] In these studies, CO was identified as the precursor of methanol, on a reaction pathway that involves surface formaldehyde and methylate as the observed intermediates.

Formic acid adsorption experiments have been performed in order to assign the two types of surface formate species observed under CO_2 and CO hydrogenation conditions. After dosing a pulse of formic acid in nitrogen carrier gas to the catalyst at room temperature, DRIFT spectra were recorded after raising the temperature by successive steps of 50 K. For comparison, amorphous ZrO_2 and an impregnated Pd/ZrO_2 catalyst have also been investigated in analogous adsorption experiments. The respective spectra recorded at 323 K are shown in Fig. 9(*a–c*). Weak shoulders around 1720 and 1200 cm^{-1} are due to physisorbed formic acid. Bidentate carbonate species formed by surface oxidation of the acid give rise to a doublet of C=O and C—O stretching vibrations at *ca.* 1650 and *ca.* 1220 cm^{-1}, respectively (*cf.* Table 1). The carbonate bands are most intense over pure zirconia (bottom trace), where, in addition, monodentate carbonate is detected (1400–1450 cm^{-1}).

Doublets of bands at 1580/1380 cm^{-1} ('type I') and 1600/1360 cm^{-1} ('type II') corresponding to surface formate appear in the spectra of all three systems. The inner doublet (1580/1380 cm^{-1}) is typical of formate adsorbed on zirconia;[4,6] in addition, the 1600 cm^{-1} band is visible as a shoulder in the spectrum on pure ZrO_2 [Fig. 9(*a*)]. On Pd/ZrO_2 and Au/ZrO_2, a superposition of both types of formate species is seen.

Desorption processes taking place when the temperature is raised subsequent to formic acid adsorption are monitored in Fig. 9(*d*) and (*e*), where differences between the spectra recorded at 473 and 423 K are presented. With Au/ZrO_2, several bands are decreasing under these conditions, *i.e.* carbonate vibrations and the doublets corresponding to both types of formate species. From Pd/ZrO_2, desorption of type I formate is predominantly observed. The desorption of both types of species from Pd/ZrO_2 is only seen with higher formate coverages, as shown in Fig. 9(*f*). For this spectrum, a pulse of HCO_2H was dosed at 453 K, and changes occurring on the surface between 2 and 15 min after addition were recorded.

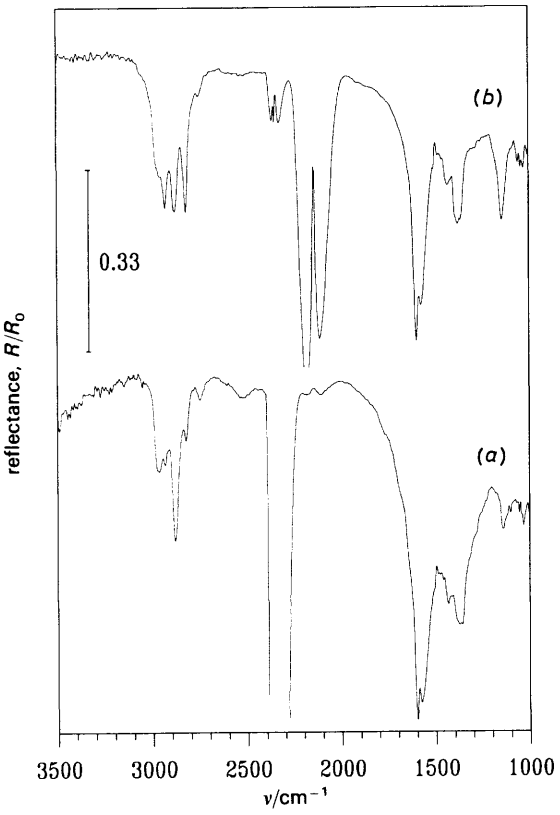

Fig. 8 Comparison of CO and CO_2 hydrogenation reactions over the 5 wt.% Au/ZrO_2 catalyst at 523 K. The catalyst is exposed to continuous flows of the respective reaction mixtures. DRIFT spectra have been recorded 15 min after the flow had been switched from pure hydrogen to a CO_2–H_2(1 : 4) reaction mixture (*a*), or to a CO–H_2 (1 : 3) reaction mixture (*b*) respectively, at a pressure of 3 bar

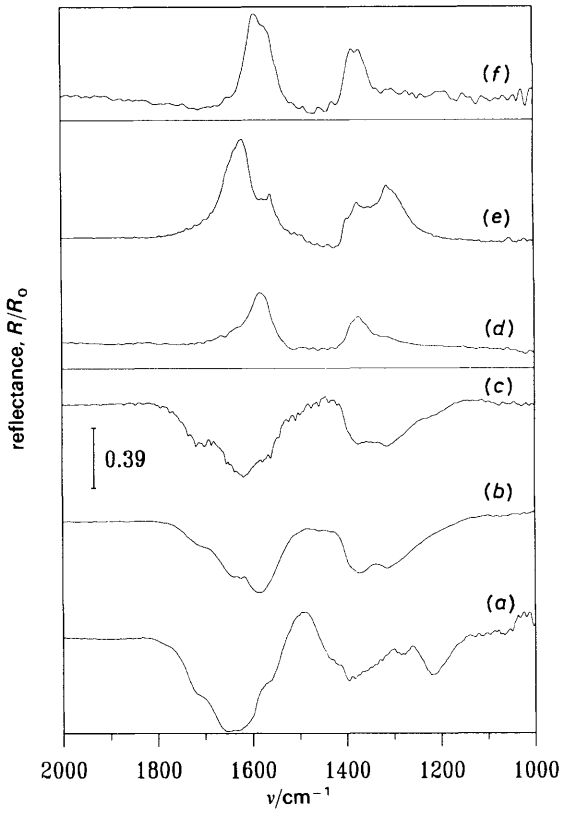

Fig. 9 Adsorption of formic acid on amorphous zirconia (*a*), Pd/ZrO_2 (*b*), and Au/ZrO_2 (*c*), surfaces. DRIFT spectra recorded at 323 K subsequent to formic acid addition at room temperature are presented in the lower panel. Desorbing species are monitored by plotting the difference between spectra recorded at 473 and 423 K (middle panel) for (*d*) Pd/ZrO_2 and (*e*) Au/ZrO_2. In the top trace, changes in the surface spectrum (Pd/ZrO_2) occurring between 2 and 15 min after HCO_2H addition at 453 K were recorded; this spectrum is plotted on a six times expanded ordinate scale (*f*)

Discussion

Catalytic tests show that the very low activity of the as-quenched amorphous $Au_{25}Zr_{75}$ alloy is due to its low intrinsic surface area, of less than 1 $m^2\ g^{-1}$. Exposure of the amorphous precursor to CO_2 hydrogenation conditions results in a transformation to the final, catalytically active state, which exhibits largely different textural and structural properties, as compared to the initial alloy. The changes occurring, *i.e.* the CO_2-induced oxidation of zirconium to zirconium dioxide, and the formation of metallic gold particles, are paralleled by a drastic increase in the CO_2 conversion rate. This process is accompanied by a conversion of the compact alloy into a porous, high surface area system.

Major factors that determine the activity increase observed during *in situ* exposure are the enlarged surface area, possible segregation of gold on the surface,[23] and the development of particular structural features.[8] A detailed differentiation of these factors requires reliable techniques to determine the specific gold surface area, which is awaiting further efforts.

Similar morphological changes during activation have been reported by Shibata *et al.*[2] for an amorphous Au–Zr alloy exposed to CO hydrogenation conditions, and by Gasser and Baiker[3] for an amorphous Cu–Zr alloy activated under the same reaction conditions as used in this work. In contrast to Cu/ZrO_2, where methanol was identified as the main hydrogenation product,[3,4] the RWGS reaction was observed to prevail on Au/ZrO_2 systems under CO_2 hydrogenation conditions, which leads to predominant CO production. For comparison, note that under CO hydrogenation conditions, Shibata *et al.*[2] have reported the formation of methane as the main reaction in the 473–523 K temperature range, with the catalysts derived from amorphous precursors showing a considerably higher activity than Au/ZrO_2 catalysts prepared by conventional impregnation techniques.

For our CO_2 hydrogenation catalysts prepared by the two different routes described above, one observes a similar selectivity pattern (Fig. 2), which indicates that the nature of the active sites is similar for both systems. The observed marked differences in CO_2 hydrogenation rates may originate from the different metal loadings of the catalysts (5 wt.% Au for the conventionally prepared catalyst, as compared with 25 at.% Au for the catalyst derived from the amorphous alloy), and from the variation of the mean gold particle size (15 and 8.5 nm, respectively). A further reason for the differences in the catalytic behaviour may be found in the nature of the zirconia phase. XRD measurements reveal the presence of monoclinic ZrO_2, with a low degree of crystallinity, for the catalyst derived from the amorphous alloy; in contrast, with the conventionally prepared catalyst a well crystallized tetragonal ZrO_2 modification is prevailing. The difference in the Au/ZrO_2 interfacial area, which results from these distinct structural properties, could be responsible for the observed variation in catalytic activity of these catalysts.

Note that calcination of the catalyst prepared by coprecipitation leads to a marked increase in the CO_2 hydrogenation rate. This contrasts the findings with Cu/ZrO_2 catalysts, where calcination of the samples resulted in a drastic decrease of the catalytic activity, probably induced by crystallization

of initially amorphous zirconia.[24] A valuable hint on the origins of the activity surge observed with Au/ZrO_2 is found in recent investigations by Haruta *et al.*[25] on the preparation of supported-gold catalysts by coprecipitation. During calcination, gold compounds were decomposed to form metallic gold crystallites, which were reported to segregate from the interior to the surface of the coprecipitate particles. Such a segregation of gold could be the reason for the increased catalytic activity observed after calcination with the coprecipitated Au/ZrO_2 catalyst used in this work; evidence for this process must be obtained by further structural investigations.

The FTIR spectroscopic results interpreted in the above section contain valuable information concerning the 'basic' RWGS reaction which we have previously discussed.[4] The CO_2 hydrogenation experiment at 403 K (Fig. 5) provides evidence for a reaction pathway in which CO is produced from bidentate surface carbonate. Possible intermediate reactions can be formulated as follows.

$$CO_2 + O^{2-}(\text{surface}) \rightarrow CO_3^{2-}$$

$$CO_3^{2-} + H_2 \rightarrow CO(g) + 2OH^-(\text{surface})$$

$$2OH^-(\text{surface}) \rightarrow H_2O(g) + O^{2-}(\text{surface}).$$

On the catalyst derived from the amorphous precursor $Au_{25}Zr_{75}$, however, rapid formation of gaseous CO without intermediate steps was observed. We therefore cannot exclude that the products of the RWGS reaction are also produced by other mechanisms. In this context the role of lattice anion vacancies should be pointed out, which are of potential importance for the prevailing mechanism: CO_2 or surface carbonate may react with one or two vacancies, respectively, to yield gaseous CO and the corresponding oxygenated zirconium sites. Anion vacancies have also been discussed in the intepretation of our results on amorphous Pd/ZrO_2 catalysts,[11] and will be the subject of further investigations.

The corresponding reverse reaction, *i.e.* the WGS reaction, is indicated by a relatively high CO_2 formation rate under CO hydrogenation conditions. This reaction is likely to proceed *via* the oxidation of CO by loosely bound oxygen or hydroxy groups from the disordered zirconia matrix.

To conclude, the influence of Au/ZrO_2 catalysts on the WGS/RWGS equilibrium is very similar to the behaviour of the Cu/ZrO_2 systems.[4] The same analogies are found with respect to the reaction scheme discussed in ref. 6. Upon exposure of the catalysts to CO_2–H_2 reaction mixtures, rapid formation of surface formate is observed. With Pd/ZrO_2 catalysts, formate has been identified as the precursor of methane.[6] On the coprecipitated Au/ZrO_2 catalysts, surface formate is also abundant but does not appear as an observable reaction intermediate, because methane is produced only at temperatures higher than those investigated in the FTIR spectroscopic experiments. A further reaction pathway presented in ref. 6 for Pd/ZrO_2 starts from CO, and leads to the methanol product *via* π-bonded formaldehyde and surface methylate; interconversions of surface species on this branch of the reaction scheme proceed more slowly than the reactions involving surface formate. Again, the results with Au/ZrO_2 are matching these conclusions: the corresponding intermediates are observed only at longer reaction times during CO_2 hydrogenation reactions, but are strongly enhanced when starting from CO–H_2.

Methylate and methanol signals are weak as compared to the respective bands observed on Cu/ZrO_2. Apparently the hydrogenation of formaldehyde-type species to methanol is less efficiently catalysed on gold, as compared with copper. As an alternative explanation for the low methanol selectivity of the Au/ZrO_2 catalyst, the possibility of consecutive decomposition of methanol on the surface cannot be ruled out.

Concerning the observed surface formate species, two features are emerging from the present experiments that deserve a short discussion, *i.e.* the very intensive combination bands observed in the 2700–3000 cm^{-1} range, and the doublet splitting of the asymmetric CO_2^- stretching vibration (<1600 cm^{-1}). Detection of combination vibrations has previously been described in the literature,[20,21] and is observed on Au/ZrO_2 owing to the unusually high coverage of surface formate. We have also observed these bands on amorphous Pd/ZrO_2 with lower intensity.[11]

The splitting of the carboxylate stretching bands implies the presence of at least two different types of formate species. These species are also observed on pure zirconia and on Pd/ZrO_2. Therefore, an assignment of either pair of bands to formate on gold is unlikely; rather, the two types of formate appear to be bound to different sites on the zirconia matrix. The spectra recorded under CO_2 hydrogenation conditions indicate that type I formate (1580/1380 cm^{-1}) is observed first. After the more reactive zirconia sites have been covered with type I species, the doublet at 1600/1360 cm^{-1} corresponding to type II formate appears to grow. The formic acid adsorption experiments reveal important differences between the three surfaces studied (Fig. 9). On pure zirconia, the concentration of type I formate, and hence the density of the more active surface sites, remains low. On Au/ZrO_2, both types of formate species are observed in significant concentration. Finally, on the Pd/ZrO_2 surface the type I formate signals are dominant. Apparently the metal is important in determining the concentration of the more reactive zirconia sites which are capable of binding type I formate species. Note that on Pd/ZrO_2, where the hydrogenation of formate to methane is very efficiently catalysed,[11] the highest concentration of type I surface formate species is observed.

This work has been supported by grants of the Schweizerische Bundesamt für Energiewirtschaft and of the Deutsche Forschungsgemeinschaft (SFB 213). One of us (Ch. S.) is grateful to the Fonds der Chemischen Industrie for a graduate research fellowship.

References

1 (*a*) A. Molnar, G. V. Smith and M. Bartok, *Adv. Catal.*, 1989, **36**, 329; (*b*) A. Baiker, *Faraday Discuss. Chem. Soc.*, 1989, **87**, 239; (*c*) A. Baiker, in *Glassy Metals 3*, ed. H. Beck and H. J. Güntherodt, Springer Verlag, Berlin, 1991, in the press.
2 M. Shibata, N. Kawata, T. Masumoto and H. Kimura, *Chem. Lett.*, 1985, 1605.
3 D. Gasser and A. Baiker, *Appl. Catal.*, 1989, **48**, 279.
4 Ch. Schild, A. Wokaun and A. Baiker, *J. Mol. Catal.*, 1990, **63**, 243.
5 A. Baiker and D. Gasser, *J. Chem. Soc., Faraday Trans. 1*, 1989, **85**, 999.
6 Ch. Schild, A. Wokaun and A. Baiker, *J. Mol. Catal.*, 1990, **63**, 223.
7 Ch. Schild, A. Wokaun, R. A. Köppel and A. Baiker, *J. Phys. Chem.*, 1991, in the press.
8 A. Baiker, D. Gasser, J. Lenzer, A. Reller and R. Schlögl, *J. Catal.*, 1990, **126**, 555.
9 E. A. Shaw, T. Rayment, A. P. Walker, J. R. Jennings and R. M. Lambert, *Catal.*, 1990, **126**, 219.
10 A. Frost, *Nature (London)*, 1988, **334**, 577.
11 Ch. Schild, A. Wokaun and A. Baiker, *J. Mol. Catal.*, 1991, in the press.
12 B. E. Warren, *J. Appl. Phys.*, 1941, **12**, B75.
13 S. J. Gregg and K. S. W. Sing, *Surf. Colloid. Sci.*, 1976, **9**, 254.
14 E. P. Barrett, L. S. Joyner and P. P. Halenda, *J. Am. Chem. Soc.*, 1951, **73**, 373.
15 G. Halsey, *J. Chem. Phys.*, 1948, **16**, 931.
16 K. S. W. Sing, D. H. Everett, R. A. W. Haul, L. Moscou, R. A. Pierotti, J. Rouquerol and T. Siemieniewska, *Pure Appl. Chem.*, 1985, **57**, 603.
17 B. V. Lippens and J. H. de Boer, *J. Catal.*, 1965, **4**, 319.

18 J. G. Chen, P. Basu, L. Ng and J. T. Yates Jr., *Surf. Sci.*, 1988, **194**, 397, and ref. therein.
19 P. Pichat, J. Veron, B. Claudel and M. V. Mathieu, *J. Chim. Phys.*, 1966, **63**, 1026.
20 V. F. Kiselev and O. V. Krylov, *Adsorption and Catalysis on Transition Metals and their Oxides*, Springer Verlag, Berlin, 1989, and ref. therein.
21 J. F. Edwards and G. L. Schrader, *J. Phys. Chem.*, 1985, **89**, 782.
22 B. E. Hayden, K. Prince, D. P. Woodruff and A. M. Bradshaw, *Phys. Rev. Lett.*, 1983, **51**, 475.
23 F. Vanini, S. Büchler, X-n. Yu, M. Erbudak, L. Schlapbach and A. Baiker, *Surf. Sci.*, 1987, **189/190**, 1117.
24 R. A. Koeppel, A. Baiker, Ch. Schild and A. Wokaun, in *Preparation of Catalysts V*, ed. B. Delmon, P. Grange, P. A. Jacobs, G. Poncelet and P. Ruiz, Elsevier, Amsterdam, 1990, p. 283.
25 M. Haruta, N. Yamada, T. Kobayashi and S. Iijima, *J. Catal.*, 1989, **115**, 301.

Paper 1/00993A; *Received 4th March*, 1991